Estimation of the fossil-fuel component in atmospheric CO_2 based on radiocarbon measurements at the Beromünster tall tower, Switzerland

Tesfaye A. Berhanu[1], Sönke Szidat[2], Dominik Brunner[3], Ece Satar[1], Rüdiger Schanda[1], Peter Nyfeler[1], Michael Battaglia[2], Martin Steinbacher[3], Samuel Hammer[4] and Markus Leuenberger[1]

[1]*Climate and Environmental Physics, Physics Institute and Oeschger Centre for Climate Change Research, University of Bern, Bern, Switzerland*

[2]*Department of Chemistry and Biochemistry and Oeschger Center for Climate Change Research, University of Bern, Bern, Switzerland*

[3]*Empa, Laboratory for Air Pollution/Environmental Technology, Dübendorf, Switzerland*

[4]*Institut für Umweltphysik, Universität Heidelberg, Heidelberg, Germany*

Abstract

Fossil fuel CO_2 (CO_{2ff}) is the major contributor of anthropogenic CO_2 in the atmosphere, and accurate quantification is essential to better understand the carbon cycle. Since October 2012, we have been continuously measuring the mixing ratios of CO, CO_2, CH_4 and H_2O at five different heights at the Beromünster tall tower, Switzerland. Air samples for radiocarbon ($\Delta^{14}CO_2$) analysis have also been collected from the highest sampling inlet (212.5 m) of the tower on a bi-weekly basis. A correction was applied for $^{14}CO_2$ emissions from nearby nuclear power plants (NPPs), which have been simulated with the Lagrangian transport model FLEXPART-COSMO. The $^{14}CO_2$ emissions from NPPs offset the depletion in ^{14}C by fossil-fuel emissions resulting in an underestimation of the fossil-fuel component in atmospheric CO_2 by about 16 %. An average observed ratio (R_{CO}) of 13.4 ± 1.3 mmol/mol was calculated from the enhancements in CO mixing ratios relative to the clean air reference site Jungfraujoch (ΔCO) and the radiocarbon-based fossil-fuel CO_2 mole fractions. The winter

time R_{CO} estimate of 12.5 ± 3.3 is about 30 % higher than the winter time ratio between in-situ measured CO and CO_2 enhancements at Beromünster over the Jungfraujoch background (8.7 mmol/mol) corrected for non-fossil contributions due to strong biospheric contribution despite the strong correlation between ΔCO and ΔCO_2 in winter. By combining the ratio derived using the radiocarbon measurements and the in-situ measured CO mixing ratios, a high-resolution time series of CO_{2ff} was calculated exhibiting a clear seasonality driven by seasonal variability in emissions and vertical mixing. By subtracting the fossil-fuel component and the large-scale background, we have determined the regional biospheric CO_2 component that is characterized by seasonal variations ranging between -15 to +30 ppm. A pronounced diurnal variation was observed during summer modulated by biospheric exchange and vertical mixing while no consistent pattern was found during winter.

1. Introduction

Fossil fuel CO_2 (CO_{2ff}) is the fundamental contributor to the increase in atmospheric CO_2, hence its precise quantification is crucial to better understand the global carbon budget. One of the major uncertainties in the projections of climate change is the uncertainty in the future carbon budget due to feedbacks between terrestrial ecosystems and climate (Heimann and Reichstein, 2008). Information on the response of the biosphere to climate variations can be obtained from atmospheric CO_2 observations, but isolating the biospheric signal in the measured CO_2 mixing ratios requires an accurate quantification of the fossil fuel component. Several methods have therefore been proposed for quantifying CO_{2ff}, which are based on observations or models. A widely employed approach is to determine CO_{2ff} with an atmospheric transport model that incorporates CO_{2ff} emissions from a bottom-up emission inventory.

Emission inventories are based on statistics of the energy-use by different sectors and the quantification of CO_{2ff} emissions by accounting for the carbon content of each fuel and its corresponding oxidation ratios (Friedlingstein et al., 2010; Le Quéré et al., 2016). When compared to other greenhouse gases, national emission inventories for CO_2 are quite accurate, but the computation of these inventories is laborious, and the quality depends on the energy statistics and reporting methods that vary strongly between countries (Marland, 2008; Marland et al., 2009). A recent study evaluating different energy statistics and cement production data estimated an uncertainty of about 5 % for the global fossil-fuel emissions of the past decade (2006 – 2015)(Le Quéré et al., 2016). At country level the uncertainties are usually below 5 % in developed countries but often exceed 10 % in developing countries (Ballantyne et al., 2015).

Additional uncertainties arise from the spatial and temporal disaggregation of national annual total emissions to the grid of the atmospheric transport model. At sub-country scales (less than 150 km), the uncertainty from bottom-up estimates can reach up to 50 % (Ciais et al., 2010). Finally, errors in the transport model and the inability to correctly represent point observations in the model may contribute substantially to the uncertainty of model simulated CO_{2ff} mixing ratios (Tolk et al., 2008; Peylin et al., 2011).

Radiocarbon measurements can be used to directly quantify CO_{2ff} in atmospheric CO_2 observations. Radiocarbon is produced in the upper atmosphere during the reaction of neutrons with nitrogen induced by cosmic rays (Currie, 2004). In addition, nuclear bomb tests in the 1960´s led to large radiocarbon input into the atmosphere which was thereafter decreasing due to gradual uptake by the oceans and the terrestrial biosphere (Manning et al., 1990; Levin et al., 2010). Nowadays, the decline in atmospheric $^{14}CO_2$ is mainly driven by input from ^{14}C-free fossil fuel CO_2 (Levin et al., 2010). This decline is well detectable at background sites such as Jungfraujoch, Switzerland and Schauinsland, Germany (Levin et al.,

2013). While all reservoirs exchanging carbon with the atmosphere are relatively rich in ^{14}C, fossil-fuels (millions of years old) are devoid of ^{14}C due to its radioactive decay with a half-life of 5370 years. Hence, any fossil-fuel CO_2 emitted to the atmosphere will dilute the background ^{14}C signal, the so-called Suess effect, which can then be used to unravel recently added fossil-fuel CO_2 to the atmosphere (Zondervan and Meijer, 1996; Levin et al., 2003; Gamnitzer et al., 2006; Turnbull et al., 2006; Levin and Karstens, 2007; Turnbull et al., 2009; Turnbull et al., 2011; Lopez et al., 2013; Turnbull et al., 2014; Turnbull et al., 2015). However, this depletion can also partially be offset by CO_2 release from the biosphere which has enriched $^{14}C/^{12}C$ ratios due to nuclear bomb tests in the 1960's. ^{14}C produced by these tests was absorbed by the land biosphere and is now gradually being released back to the atmosphere (Naegler and Levin, 2009). Another contribution could be direct ^{14}C emissions from nuclear industries (Levin et al., 2010) . This technique also enables separation between biospheric and fossil-fuel CO_2 components in atmospheric CO_2 observations, and thus better constrains the biospheric CO_2 fluxes when coupled with inversion models (Basu et al., 2016). The uncertainty in CO_{2ff} estimated by the radiocarbon method is mainly determined by the precision in the ^{14}C measurement, the choice of background as well as the uncertainty in the contribution from other sources of ^{14}C such as nuclear power plants (NPPs) (Turnbull et al., 2009).

Despite its importance as a fossil-fuel tracer, measurements of ^{14}C are still sparse. The measurements are expensive and laborious, which so far has prevented frequent sampling and has motivated researchers to combine ^{14}C measurements with additional tracers such as CO to enhance spatial and temporal coverage (Gamnitzer et al., 2006; Turnbull et al., 2006; Levin and Karstens, 2007; Vogel et al., 2010; Turnbull et al., 2011; Lopez et al., 2013; Turnbull et al., 2014; Turnbull et al., 2015). The CO-method relies on using high frequency CO measurements and regular calibration of the temporally changing $\Delta CO:\Delta CO_{2ff}$ ratios based on

weekly or bi-weekly ^{14}C measurements. Despite its advantage of providing a proxy for continuous CO_{2ff} data, the method introduces additional uncertainties due to diurnal and seasonal variability in the CO sink, and the presence of multiple non-fossil CO sources such as oxidation of hydrocarbons or wood and biofuel combustion (Gamnitzer et al., 2006). Spatial variations in the $\Delta CO:\Delta CO_2$ ratio across Europe due to different source compositions and environmental regulations, which affects the measured ratios due to changes in air mass origin (Oney et al., 2017) are the main reason for the temporally changing $\Delta CO:\Delta CO_{2ff}$ ratio for a given measurement site. Additionally, variability in the CO/CO_2 emission ratios of the sources can contribute to its spatial and temporal variability (Vogel et al., 2010; Turnbull et al., 2015).

In Switzerland, CO_2 contributes about 82 % of the total greenhouse gas emissions according to the Swiss national emission inventory for 2013, and fossil-fuel combustion from the energy sector contributes more than 80 % of the total CO_2 emission (FOEN, 2015b). In order to validate such bottom-up estimates, independent techniques based on atmospheric measurements are desirable. In addition, as mentioned above, the biospheric CO_2 signals can only be estimated with a good knowledge of CO_{2ff}. In this study, we present and discuss $^{14}CO_2$ measurements conducted bi-weekly between 2013 and 2015 at the Beromünster tall tower in Switzerland. From these samples in combination with background CO, CO_2 and $^{14}CO_2$ measurements at the high-altitude remote location Jungfraujoch, Switzerland, ΔCO to ΔCO_{2ff} ratios (R_{CO}) are derived. These ratios are then combined with the in-situ measured ΔCO mixing ratios to estimate a high-resolution time series of atmospheric CO_{2ff} mixing ratios, and by difference, of the biospheric CO_2 component. The influence of ^{14}C emissions from nearby NPPs and correction strategies are also discussed.

2. Methods

2.1. Site description and continuous measurement of CO and CO_2

A detailed description of the Beromünster tall tower measurement system as well as a characterization of the site with respect to local meteorological conditions, seasonal and diurnal variations of greenhouse gases, and regional representativeness can be obtained from previous publications (Oney et al., 2015; Berhanu et al., 2016; Satar et al., 2016). In brief, the tower is located near the southern border of the Swiss Plateau, the comparatively flat part of Switzerland between the Alps in the south and the Jura mountains in the northwest (47° 11′ 23″ N, 8° 10’ 32″ E, 797 m a.s.l.), which is characterized by intense agriculture and rather high population density (Fig. 1). The tower is 217.5 m tall with access to five sampling heights (12.5 m, 44.6 m, 71.5 m, 131.6 m, 212.5 m) for measuring CO, CO_2, CH_4 and H_2O using Cavity Ring Down Spectroscopy (CRDS) (Picarro Inc., G-2401). By sequentially switching from the highest to the lowest level, mixing ratios of these trace gases were recorded continuously for three minutes per height, but only the last 60 seconds were retained for data analysis. The calibration procedure for ambient air includes measurements of reference gases with high and low mixing ratios traceable to international standards (WMO-X2007 for CO_2 and WMO-X2004 for CO and CH_4), as well as target gas and more frequent working gas determinations to ensure the quality of the measurement system. From two years of data a long-term reproducibility of 2.79 ppb, 0.05 ppm, and 0.29 ppb for CO, CO_2 and CH_4, respectively was determined for this system (Berhanu et al., 2016).

2.2. Sampling and CO_2 extraction for isotope analysis

Air samples for $^{14}CO_2$ analysis were collected from the highest inlet usually between 9:00 to 13:00 UTC. At the beginning we collected one sample per month which was eventually changed to every second week sampling from November 2013 onwards. During each sampling event, three samples were collected over a 15-minute interval in 100 L PE-AL-PE bags (TESSERAUX, Germany) from the flush pump exhaust line of the 212.5 m sampling inlet, which has a flow rate of about 9 L min^{-1} at ambient conditions. The sampling interval

was chosen to ensure radiocarbon sample collection in parallel with the continuous CO and CO_2 measurements by the CRDS analyzer at the highest level. Each bag was filled at ambient air pressure for 6 to 8 minutes and a total air volume of 50 to 70 L (at STP) was collected.

CO_2 extraction was conducted cryogenically in the laboratory at the University of Bern usually the day after the sample collection. During the extraction step, the air sample was first pumped through a stainless steel water trap (-75 °C), which was filled with glass beads (Rashig rings, 5 mm, Germany). A flow controller (Analyt-MTC, Aalborg, USA) with flow totalizer tool was attached to this trap to maintain a constant flow of air (1.2 L min^{-1}) towards the second trap (trap 2), a spiral-shaped stainless steel tube (1/4") filled with glass beads (~ 2 mm) and immersed in liquid nitrogen to freeze out CO_2. When the flow ceased, trap 2 was isolated from the line and evacuated to remove gases which are non-condensable at this temperature. Then, trap 2 was warmed to room temperature, and eventually immersed in slush at -75 °C to freeze out any remaining water. Finally, the extracted CO_2 was expanded and collected in a 50 mL glass flask immersed in liquid nitrogen.

Sample extraction efficiency was calculated by comparing the amount of the cryogenically extracted CO_2 with the CO_2 measured in-situ by the CRDS analyzer during the time of sampling. The amount of CO_2 extracted is determined first by transferring the extracted CO_2 cryogenically to a vacuum line of predetermined volume. Then, based on the pressure reading of the expanded gas, and the total volume of air collected determined by the mass flow controller with a totalizer function attached to trap 1, CO_2 mixing ratios were calculated.

At the end of 2014 we noticed that there was a leakage from the sampling line exhaust pumps, which resulted in unrealistically high CO_2 mixing ratios (usually more than 500 ppm). Therefore, we replaced all the exhaust pumps and to further ensure that the leakage problem during sampling is solved, we regularly check for leaks before sampling by closing the needle

valves leading to the pumps and monitoring in case there is any flow with the flow meter attached after the pump. Since the replacement we have not observed any indication of leakage. Seven samples, which were suspected to be contaminated due to this issue, were consequently excluded. The sample extraction efficiency since then has usually been better than 99 %. We also made a blank test to check the presence of any leaks or contamination during sample processing but did not observe any of these issues. Five more samples were excluded in 2014 due to a strong mismatch among triplicates in the measured CO_2 after the sample extraction which indicated contamination.

2.3. Measurement of $\delta^{13}C$, $\delta^{18}O$ and $\Delta^{14}C$

Prior to radiocarbon measurement, the extracted CO_2 was analyzed for the stable isotopes $\delta^{13}C$ and $\delta^{18}O$ using the Isotope Ratio Mass Spectrometer (IRMS, Finnigan MAT 250) at the Climate and Environmental Physics Division of University of Bern, which has an accuracy and precision of better than 0.1 ‰ for both $\delta^{13}C$ and $\delta^{18}O$ (Leuenberger et al., 2003). ^{14}C analysis of the extracted CO_2 was performed with an accelerator mass spectrometer (AMS) MICADAS (MIni CArbon DAting System) at the Laboratory for the Analysis of Radiocarbon (LARA) at the Department of Chemistry and Biochemistry of the University of Bern (Szidat et al., 2014). An automated graphitization equipment (AGE) was used to prepare solid target gas (Nemec et al., 2010) from the extracted CO_2 stored in 50 mL glass flasks. A measurement series consisted of up to 15 air samples converted to 30 solid graphite targets (duplicates), together with four and three targets from CO_2 produced by combustion of the NIST standard oxalic acid II (SRM 4990C) and fossil CO_2 (Carbagas, Gümligen), respectively, which were used for the blank subtraction, standard normalization, and correction for isotopic fractionations. For the fractionation correction, $\delta^{13}C$ values of the AMS were used, which show a long-term standard uncertainty of ± 1.2 ‰ (Szidat et al., 2014). The

198 AMS $\delta^{13}C$ values agree well on average with the corresponding IRMS results, revealing a
199 statistically insignificant difference of -0.2 ± 1.2 ‰ with slightly more depleted AMS results.
200 Data reduction was performed using the BATS program (Wacker et al., 2010). The
201 uncertainty of an individual ^{14}C measurement typically amounts to ~2.1 ‰, including
202 contributions from counting statistics (~1.1 ‰), corrections of normalization (*i.e.* blank
203 subtraction, standard normalization, and correction for isotopic fractionations) (~1.1 ‰) and
204 an unaccounted long-term variability of sampling and ^{14}C analysis according to Szidat et al.,
205 2014 (1.5 ‰), contributions comparable to previous observations (Graven et al., 2007).
206 During calculation of weighted averages of the duplicates, the uncertainty of the mean
207 is determined with the contributions of the counting statistics and the normalization, whereas
208 the uncertainty of the unaccounted long-term variability is considered fully afterwards, as this
209 contribution cannot be reduced by averaging of two measurements performed on the same
210 day. This uncertainty of the weighted average typically amounts to ~1.9 ‰; it is compared
211 with the standard deviation of the duplicates and the larger of these values is used as the final
212 uncertainty of the duplicates. The mean of the three individual samples from the same day,
213 which is used below in Section 2.4.1 as $\Delta^{14}C_{meas}$, is then determined and associated with the
214 average uncertainty of the three duplicates, as the variability of the three samples is
215 comparable to this average uncertainty for all cases.
216 As $^{14}C/^{12}C$ from Beromünster was measured at the LARA laboratory in Bern, whereas
217 the corresponding background samples from Jungfraujoch were analyzed at the low-level
218 counting (LLC) facility of the Institute of Environmental Physics, Heidelberg University, the
219 datasets needed to be adjusted to each other. A recent interlaboratory compatibility test
220 between the LARA lab (code #2) and Heidelberg (LLC) estimated a small bias (Hammer et
221 al., 2016). The measurement bias (*i.e.* the mean difference of the measured $\Delta^{14}C$ minus the
222 consensus value of the participating laboratories for all investigated CO_2 samples) is +1.8 ±

0.1 ‰ and -0.3 ± 0.5 ‰ for Bern and Heidelberg, respectively, from which the bias between both labs of 2.1 ± 0.5 ‰ is determined with a larger measured $\Delta^{14}C$ for Bern. Consequently, 2.1 ± 0.5 ‰ was subtracted from the ^{14}C measurements of the Beromünster samples.

2.4. Determination of the fossil fuel CO_2 component

2.4.1. The $\Delta^{14}C$ technique

For the determination of the CO_{2ff} component we followed similar approaches as in previous studies (Zondervan and Meijer, 1996; Levin et al., 2003; Levin and Karstens, 2007; Turnbull et al., 2009). The measured CO_2 is assumed to be composed of three major components: the free troposphere background (CO_{2bg}), the regional biospheric component (CO_{2bio}) comprising photosynthesis and respiration components, and the fossil-fuel component (CO_{2ff}):

$$CO_{2meas} = CO_{2bg} + CO_{2bio} + CO_{2ff} \quad (1)$$

Each of these components has a specific $\Delta^{14}C$ value (i.e. the deviation in per mil of the $^{14}C/^{12}C$ ratio from its primary standard, and corrected for fractionation and decay using ^{13}C measurements) described as $\Delta^{14}C_{meas}$, $\Delta^{14}C_{bg}$, $\Delta^{14}C_{bio}$ and $\Delta^{14}C_{ff}$. In analogy to Eq. (1), a mass balance approximation equation can also be formulated for ^{14}C as:

$$CO_{2meas}\,(\Delta^{14}C_{meas} + 1000\ ‰) = CO_{2bg}\,(\Delta^{14}C_{bg} + 1000\ ‰) + CO_{2bio}\,(\Delta^{14}C_{bio} + 1000\ ‰) + CO_{2ff}\,(\Delta^{14}C_{ff} + 1000\ ‰) \quad (2)$$

Note that non-fossil fuel components such as biofuels are incorporated into the biospheric component in Eq. (1). The fossil-fuel term in Eq. (2) is zero as fossil fuels are devoid of radiocarbon ($\Delta^{14}C_{ff}$ = -1000 ‰). Replacing the biospheric CO_2 component in Eq. (1) by a formulation derived from Eq. (2), the fossil fuel CO_2 component is derived as:

$$CO_{2ff} = \frac{CO_{2bg}\left(\Delta^{14}C_{bg} - \Delta^{14}C_{bio}\right) - CO_{2meas}\,(\Delta^{14}C_{meas} - \Delta^{14}C_{bio})}{\Delta^{14}C_{bio} + 1000‰} \quad (3)$$

Equation (3) can be further simplified by assuming that $\Delta^{14}C_{bio}$ is equal to $\Delta^{14}C_{bg}$ (Levin et al., 2003) as:

$$CO_{2ff} = \frac{CO_{2meas}(\Delta^{14}C_{bg} - \Delta^{14}C_{meas})}{\Delta^{14}C_{bg} + 1000‰} \quad (4)$$

Hence, the fossil fuel CO_2 component can be determined using the CO_{2meas} and $\Delta^{14}C_{meas}$ values measured at the site as well as $\Delta^{14}C_{bg}$ obtained from the Jungfraujoch mountain background site in the Swiss Alps.

However, the CO_{2ff} determined using Eq. (4) incorporates a small bias due to the non-negligible disequilibrium contribution of heterotrophic respiration as well as due to contributions from NPPs. To correct for the bias from these other contributions, an additional term (CO_{2other} and $\Delta^{14}C_{other}$) can be included in Eq. (4) as suggested by Turnbull et al. (2009):

$$CO_{2ff} = \frac{CO_{2meas}(\Delta^{14}C_{bg} - \Delta^{14}C_{meas})}{\Delta^{14}C_{bg} + 1000‰} + \frac{CO_{2other}(\Delta^{14}C_{other} - \Delta^{14}C_{bg})}{\Delta^{14}C_{bg} + 1000‰} \quad (5)$$

where CO_{2other} and $\Delta^{14}C_{other}$ represent the additional CO_2 and radiocarbon contributions from other sources such as NPPS and biospheric fluxes, respectively.

The contributions from heterotrophic respiration will lead to an underestimation of CO_{2ff} on average by 0.2 ppm in winter and 0.5 ppm in summer, respectively, estimated for the northern hemisphere using a mean terrestrial carbon residence time of 10 years (Turnbull et al., 2006).

To account for the bias from heterotrophic respiration, a harmonic function varying seasonally between these values was added to the derived CO_{2ff} values. However, variation of respiration fluxes on shorter timescales cannot be accounted for by this simple correction. The correction strategy for the contribution from NPPs is described in section 2.4.2 below.

2.4.2. Simulation of $^{14}CO_2$ from nuclear power plants

Radiocarbon is produced by nuclear reactions in NPPs and primarily emitted in the form of $^{14}CO_2$ (Yim and Caron, 2006), except for Pressurized Water Reactors (PWR), which release ^{14}C mainly in the form of $^{14}CH_4$. Previous studies have shown that such emissions can lead to large-scale gradients in atmospheric $\Delta^{14}C$ activity and offset the depletion from fossil-fuel emissions (Graven and Gruber, 2011). At Heidelberg in Germany, an offset of 25 % and 10 % of the fossil-fuel signal was observed during summer and winter, respectively, due to emissions from a nearby plant (Levin et al., 2003). Similarly, Vogel et al. (2013) determined the influence of NPPs for a measurement site in Canada, and estimated that about 56 % of the total CO_{2ff} component was masked by the contribution from NPPs, though this large number was obtained for a site in close vicinity of CANadian Deutrium Uranium-type reactor (CANDU) known for producing particularly high ^{14}C emissions. In Switzerland, there are five NPPs and the closest plant is located about 30 km to the northwest of Beromünster (Fig. 1). Furthermore, air masses arriving at Beromünster are frequently advected from France, which is the largest producer of nuclear power in Europe.

To estimate the influence of Swiss and other European NPPs on $\Delta^{14}C$ at Beromünster, we used FLEXPART-COSMO backward Lagrangian particle dispersion simulations (Henne et al., 2016). FLEXPART-COSMO was driven by hourly operational analyses of the non-hydrostatic numerical weather prediction model COSMO provided by the Swiss weather service MeteoSwiss at approximately 7 x 7 km^2 resolution for a domain covering large parts of Western Europe from the southern tip of Spain to the northern tip of Denmark and from the west coast of Ireland to eastern Poland. For each 3-hour measurement interval during the three-year period, a source sensitivity map (footprint) was calculated by tracing the paths of 50'000 particles released from Beromünster at 212 m above ground over 4 days backward in time. The source sensitivities were then multiplied with the $^{14}CO_2$ emissions of all NPPs within the model domain. Thereby, the emission of a given NPP was distributed over the area

of the model grid cell containing the NPP. Source sensitivities were calculated for three different vertical layers (0-50 m, 50-200 m, 200-500 m). Since the height of ventilation chimneys of the Swiss NPPs is between 99 m and 120 m, only the sensitivity of the middle layer was selected here as it corresponds best to the effective release height.

The release of ^{14}C both in inorganic (CO_2) and organic form (CH_4) is routinely measured at all Swiss NPPs. Annual totals of ^{14}C emissions are published in the annual reports of the Swiss Federal Nuclear Safety Inspectorate ENSI (https://www.ensi.ch/de/dokumente/document-category/strahlenschutzberichte/). The corresponding data have been kindly provided by the Swiss Federal Nuclear Safety Inspectorate (ENSI) and the Berner Kraftwerke (BKW) operating the NPP Mühleberg at temporal resolutions ranging from annual (Benznau 1 & 2), to monthly (Leibstadt, Gösgen), and bi-weekly (Mühleberg), and we assumed constant emissions over the corresponding periods. For Beznau 1, the emissions of 2015 were distributed over the first 3 months of the year due to the shut-down of the plant in March 2015. The largest sources of $^{14}CO_2$ in Switzerland are the two Boiling Water Reactors (BWP) Mühleberg and Leibstadt (Loosli and Oeschger, 1989). Beznau 1 & 2 and Gösgen are PWRs emitting about one order of magnitude less $^{14}CO_2$. For NPPs outside Switzerland, the emissions were estimated from energy production data reported to the International Atomic Energy Agency (IAEA) and NPP type-specific emission factors following Graven and Gruber (2011). The difference $\delta\Delta^{14}C_{nucBRM}$ in $\Delta^{14}C$ between the nuclear emission signals at Beromünster ($\Delta^{14}C_{nucBRM}$) and at Jungfraujcoh ($\Delta^{14}C_{nucJFJ}$) was then computed following Eq. (4) in Levin et al. (2010) and assuming that the mole fraction (n^{14}) of ^{14}C due to NPPs at Jungfraujoch is negligible compared to Beromünster. We then obtain:

$$\Delta^{14}C_{nuc} = f \frac{n^{14}_{app}}{n_{meas}} + 1000 \quad (6)$$

with the dimensionless factor f = 8.19 × 10_{14} and $n^{14}_{npp}/n^{CO2}_{meas}$ being the number of ^{14}C atoms due to NPPs simulated with FLEXPART-COSMO relative to total number of C-atoms (^{12}C + ^{13}C + ^{14}C) (which is equal to the total number of CO_2 molecules) measured at Beromünster.

2.4.3. Calculation of R_{CO}, $\Delta CO/\Delta CO_2$ and high resolution CO_{2ff}

A ΔCO to ΔCO_{2ff} ratio (R_{CO}) was calculated as the slope of the geometric mean regression (model II), with ΔCO being the CO enhancement over a background measured at Jungfraujoch, and the CO_{2ff} values as determined above. The CO measurements at Jungfraujoch were conducted using a CRDS analyzer (Picarro Inc., G-2401) with a measurement precision of ±2.5 ppb for 1-minute aggregates (Zellweger et al., 2012).

As CO is usually co-emitted with CO_2 during incomplete combustion of fossil and other fuels, we have also computed a tracer ratio designated as $\Delta CO/\Delta CO_2$ from the enhancements in the in-situ measured CO and CO_2 mixing ratios over the Jungfraujoch background (Oney et al., 2017). CO_{2bg} and CO_{bg} values were obtained by applying the robust extraction of baseline signal (REBS) statistical method (Ruckstuhl et al., 2012) to the continuous CO_2 and CO measurements at the high altitude site Jungfraujoch (Schibig et al., 2016) with a band width of 60 days. Note that while R_{CO} strictly refers to the ratio of ΔCO to fossil fuel CO_2 emissions, the $\Delta CO/\Delta CO_2$ ratio can be influenced by biospheric contribution as well as CO_2 emissions from non-fossil sources such as biofuels and biomass burning.

In order to construct the high resolution CO_{2ff} time series, we combined the in-situ measured CO enhancements at the Beromünster tower with the radiocarbon-derived ratios R_{CO}, and estimated CO_{2ff}^{CO} for the three-year dataset as:

$$CO_{2ff}{}^{CO} = \frac{CO_{obs} - CO_{bg}}{R_{CO}} \quad (7)$$

where CO_{obs} is the hourly averaged CO measurements at the tower.

3. Results and Discussions

3.1. $\Delta^{14}CO_2$ and CO_{2ff}

Figure 2a shows the in-situ measured hourly mean CO_2 dry air mole fractions at Beromünster (black) from the 212.5 m sample inlet matching at hours when air samples were collected for radiocarbon analysis and the corresponding background CO_2 at Jungfraujoch (blue). During the measurement period, we have recorded CO_2 mixing ratios between 389 ppm and 417 ppm. Spikes of CO_2 were observed mainly during winter, associated with weak vertical mixing and enhanced anthropogenic emissions while lower CO_2 mixing ratios were recorded during summer due to strong vertical mixing and photosynthetic uptake.

Isotopic analysis of the air samples yielded $\Delta^{14}C_{meas}$ between -12.3 ‰ and +22.8 ‰, with no clear seasonal trend, after correction for the model-simulated contribution from NPPs (Fig. 2b). Based on the simulations described in section 2.4.2, we have calculated a mean enhancement in $\Delta^{14}C$ of +1.6 ‰ and a maximum of +8.4 ‰ due to NPPs. This agrees qualitatively with the coarse resolution simulations of Graven and Gruber (2011), which suggest a mean enhancement of +1.4 ‰ to +2.8 ‰ over this region (Graven and Gruber, 2011). While about 70 % of this contribution is due to Swiss NPPs, the remaining contribution is of foreign origin. About 75 % of the contribution from the Swiss NPPs is due to Mühleberg, which is located west of Beromünster and hence frequently upstream of the site, due to the prevailing westerly winds (Oney et al., 2015). Note that each data point represents a mean value of the triplicate samples collected consecutively with a standard error of 2 ‰ among triplicates. During this period, the background $\Delta^{14}C$ values measured at Jungfraujoch varied between 15 ‰ and 28 ‰. Regional depletions in $\Delta^{14}C$ due to fossil-fuel

emissions, i.e. differences between Beromünster and the clean air reference site Jungfraujoch, were in the range of -0.7 ‰ to -29.9 ‰ with a mean value of -9.9 ‰.

Figure 2c shows the corresponding CO_{2ff} determined after correcting for radiocarbon emissions from NPPs. The typical uncertainty in CO_{2ff} is 1.2 ppm calculated by quadratically combining a mean $\Delta^{14}C$ measurement uncertainty of 2.0 ‰ in both the sample and the background values, 0.3 ‰ from biospheric correction, 0.5 ‰ from interlaboratory offset and a mean uncertainty of 1.2 ‰ in the estimation of ^{14}C contribution from NPPs. A mean fossil-fuel CO_2 contribution of 4.3 ppm was calculated from these samples. Few cases, notably the sample from 27 March 2014, showed a higher CO_{2ff} and a strong depletion in $\Delta^{14}C_{meas}$, consistent with the high CO_2 mixing ratio shown in the top panel. This can be due to a strong local fossil-fuel contribution or a polluted air mass transported from other regions of Europe coinciding with the grab samplings. As this event occurred during a period with moderate temperatures (mean temperature of 6.8 °C measured at the highest level of the Beromünster tower between March and May), strong fossil fuel CO_2 emissions due to heating are not expected. The FLEXPART-COSMO transport simulations for this event suggest an air mass origin from southeastern Europe (see supplementary materials). Periods with winds from the east, colloquially known as Bise, are well known to be associated with very stable boundary layers and correspondingly strong accumulation of air pollutants during the cold months of the year between autumn and spring. Air masses reaching Beromünster from Eastern Europe have recently been reported to contain unusually high levels of CO during late winter and early spring periods, coinciding with this sampling period (Oney et al., 2017).

By subtracting the background and fossil-fuel CO_2 contributions from the measured mixing ratios, CO_{2bio} values were also determined ranging between +11.2 ppm and -12.4 ppm (Figure 2d). Even if there is no clear seasonal trend, the lowest CO_{2bio} values were recorded during summer implying net photosynthetic CO_2 uptake while most of the values in winter are

positive or close to zero due to respiration. During summer 2015, we observed strong variability in both CO_2 and CO_{2bio} (Figs. 2a and 2d). However, this period was one of the hottest and driest summers in central Europe (Orth et al., 2016). In Switzerland, it was the second hottest summer since the beginning of measurements in 1864 with most of the extreme dates in July (MeteoSuisse, 2015). Such climate extremes can lead to enhanced respiration and reduced photosynthesis, in turn, higher CO_2 and CO_{2bio} in the atmosphere. Looking specifically at the two data points in June and July 2015, the daily average temperatures recorded at Beromünster were 24.6 °C and 26 °C at the highest inlet of 212.5 m (Fig. 2e). Based on measurements at Beromünster and other cities of the CarboCount CH network in 2013, Oney et al. (2017) reported that for a daily mean temperature of greater than 20 °C, the biosphere over the Swiss plateau tends to become a net CO_2 source. The observed positive spikes in CO_2 (Fig. 2a) and CO_{2bio} (Fig. 2d) likely resulted from such extremes.

3.2. R_{CO} values from radiocarbon measurements

From the simultaneous CO and radiocarbon measurements, we calculated an R_{CO} of 13.4 ± 1.3 mmol CO/mol CO_2 with a correlation coefficient (r^2) of 0.7, and a median value of 11.2 mmol CO/mol CO_2 (Note that change in R_{CO} is insignificant in case we use smoothed ^{14}C background from Jungfraujoch). If we split the data seasonally, R_{CO} values of 12.5 ± 3.3 mmol CO/mol CO_2 and 14.1 ± 4.0 mmol CO/mol CO_2 were obtained during winter and summer, respectively (Table 1). Even if the two values are not significantly different considering the uncertainties, the very low correlation coefficient during summer (r^2 = 0.3) imply a larger uncertainty in the derived R_{CO}. Our wintertime estimate is well within the range of values from previous studies (10-15 mmol/mol) observed at other sites in Europe and North America (Gamnitzer et al., 2006; Vogel et al., 2010; Turnbull et al., 2011). To test the sensitivity of this ratio to the selection of background site, we additionally calculated R_{CO} using background values estimated with the REBS method from the in-situ CO measurements

at Beromünster instead of Jungfraujoch. The value obtained in this way (12.7 ± 1.2, r^2 = 0.6) is not significantly different from the value obtained using Jungfraujoch as background site. Considering the persistent decrease in CO emissions (Zellweger et al., 2009) in response to the European emission legislation, our estimated R_{CO} is surprisingly high. A recent study investigating the CO to CO_2 ratio from road traffic in Islisberg tunnel, Switzerland also observed a significant decrease in this ratio comparing to previous estimates pointing to a substantial reduction in CO emissions from road traffic with a CO/CO_2 ratio of 4.15 ± 0.34 ppb/ppm (Popa et al., 2014). This may indicate a significant contribution from non-road traffic emissions, which account for more than 70 % of the total CO_2 emissions leading to the high apparent R_{CO}.

The R_{CO} value derived in this study is significantly higher than the anthropogenic CO to CO_2 emission ratio of 7.8 mmol/mol calculated from Switzerland's greenhouse gas inventory report for 2013 (FOEN, 2015b, a). However, this can be due to enhanced CO emissions transported from other European cities towards Beromünster. Oney et al. (2017) observed particularly large CO/CO_2 ratios at Beromünster during several pollution events in late winter and early spring 2013 which were associated with air mass transport from eastern Europe where poorly controlled combustion of biofuels and coal likely results in high ratios.

3.3. $\Delta CO/\Delta CO_2$ from continuous measurements

Figure 3 shows the seasonally resolved ΔCO to ΔCO_2 correlations derived from in-situ measured CO and CO_2 enhancements over the background observed at Jungfraujoch, for which we estimated a tracer ratio of 8.3 ± 0.1 mmol/mol (r^2 = 0.5) for the entire measurement period. Considering the seasonally resolved $\Delta CO/\Delta CO_2$ ratios, barely any correlation is observed in summer and weak correlations (r^2 < 0.4) during spring and autumn. This can be due to the dominance of biogenic fluxes over fossil fuel fluxes during these periods of the year. From measurements during winter, when the two species are most strongly correlated, a

440 $\Delta CO/\Delta CO_2$ ratio of 7.3 ± 0.1 mmol/mol (r^2 = 0.9) is obtained. Recently, Oney et al. (2017)
441 reported a higher wintertime ratio of 8.3 mmol/mol for the same combination of
442 measurements at Beromünster and Jungfraujoch but for a different time period. If we consider
443 only winter 2013 as in their data, we obtain essentially the same value, while much lower
444 ratios of 6.5 mmol/mol and 6.4 mmol/mol were calculated for 2014 and 2015, respectively.
445 The higher ratios in winter 2013 are likely related to the unusually cold conditions and
446 extended periods of air mass transport from Eastern Europe. Note that, in contrast to R_{CO},
447 these enhancement ratios also include emissions from non-fossil sources such as biofuels and
448 biomass burning as well as the influence of biogenic fluxes. The Swiss national inventory
449 attributes about 15 % of total CO_2 emissions in 2014 to non-fossil fuel sources (FOEN,
450 2015b). If we correct for these sources assuming a constant contribution throughout the year,
451 the winter time $\Delta CO/\Delta CO_2$ ratio for the three year data becomes 8.7 mmol/mol.

452 This ratio of 8.7 mmol/mol is still about 30 % lower than the R_{CO} estimate for the
453 same period of 12.5 mmol/mol shown as a black line in Fig. 3. This suggests that despite the
454 strong correlation between ΔCO and ΔCO_2 in winter the regional CO_2 enhancements are not
455 only caused by anthropogenic emissions but include a significant contribution from biospheric
456 respiration. Miller et al. (2012) showed that such strong correlations between CO_2 and CO
457 during winter may arise from respiratory fluxes co-located with fossil fuel fluxes trapped
458 under the wintertime shallow and stable boundary layer but with strongly biased ratios when
459 compared to R_{CO}. Turnbull et al. (2011b) also observed a substantial contribution of
460 biospheric CO_2 fluxes even during winter (20 – 30 % from non-fossil fuel sources including
461 photosynthesis and respiration) from samples collected at two sites in East Asia. The
462 magnitude of these fluxes was roughly similar to the CO_{2ff} flux when continental background
463 was used (Turnbull et al., 2015). Hence, the observed correlation between ΔCO and ΔCO_2 in
464 this study is not only due to spatially and temporally correlated sources but is caused to a

large extent by meteorological variability associated with more or less accumulation of trace gases in the boundary layer irrespective of their sources. This interpretation is also supported by the fact that a strong correlation ($r^2 > 0.7$) was also observed between CO and CH_4 during winter at the same tower site (Satar et al., 2016) despite their sources being vastly distinct. In Switzerland about 80 % of CH_4 emissions are from agriculture (mainly from ruminants) while more than 85 % of CO emissions are from the transport sector and residential heating (FOEN, 2015a).

3.4. High resolution time series of CO_{2ff} and CO_{2bio}

Figure 4 shows the hourly mean CO mixing ratios at Jungfraujoch and Beromünster between 2013 and 2015. CO mixing ratios as high as 480 ppb were recorded at Beromünster while generally lower CO values were recorded at the more remote site Jungfraujoch. A pronounced seasonality in CO can be observed at Beromünster with higher values in winter and lower values during summer due to stronger vertical mixing and chemical depletion of CO by OH (Satar et al., 2016). The hourly mean CO_{2ff} time series calculated using these continuous CO measurements and the seasonally resolved R_{CO} values derived using the radiocarbon measurements are displayed in Fig. 4c. A seasonal trend in the calculated CO_{2ff} is observed with frequent spikes of CO_{2ff} during winter while summer values show less variability. We calculated a monthly mean amplitude (peak-to-trough) of 6.3 ppm with a maximum in February and a minimum in July. During the measurement period, we have observed CO_{2ff} mixing ratios ranging up to 27 ppm coinciding with cold periods and likely from enhanced anthropogenic emissions due to heating. Instances of slightly negative CO_{2ff} contributions, which occurred during less than 5 % of the time, were associated with negative enhancements in CO (i.e. $\Delta CO < 0$). This could be simply due to an overestimation of background values by the REBS function during these periods.

Figure 5a shows the hourly averaged residual CO_{2bio} values which exhibit a clear seasonal cycle but also a considerable scatter in all seasons ranging from -13 ppm to +30 ppm. During winter, most values were close to zero or positive, implying a dominance of respiration fluxes. In summer, conversely, pronounced negative and positive excursions were observed mostly due to the diurnal cycle in net CO_2 fluxes, which are dominated by photosynthetic uptake during daytime and respiration at night. Another factor contributing to such variations may be the application of a constant emission ratio neglecting any diurnal variability (Vogel et al., 2010).

It should also be noted that any non-fossil fuel CO_2 sources such as emissions from biofuels would be incorporated into the CO_{2bio} term since CO_{2ff} in Eq. (1) represents the fossil-fuel sources only, adding more variability to the data set. In order to reduce the influence of these diurnal factors, we have looked into afternoon CO_{2bio} values (12:00 - 15:00 UTC), when the CO_2 mixing ratios along the tower are uniform (Satar et al., 2016) and R_{CO} variability is minimal. Similar to the seasonal pattern in Fig. 5a, a clear seasonal cycle in biospheric CO_2 can be observed (Fig. 5b) in agreement with biospheric exchange, but both positive and negative extremes are less frequently observed (-12 ppm to +22 ppm).

The variation in CO_{2bio} during afternoon (12:00 – 15:00 UTC) was recently estimated at this site to a range of -20 ppm to +20 ppm by combining observations and model simulations for the year 2013 (Oney et al., 2017). Our estimates are more positive when compared to their study, due to the higher R_{CO} which results in lower CO_{2ff} and correspondingly higher CO_{2bio} values.

Biospheric CO_2 shows a seasonally dependent diurnal variation as shown in Fig. 6. During winter (Dec - Feb), the biospheric CO_2 component remains consistently positive (+2 to +5 ppm) throughout the day, implying net respiration fluxes. In summer, a clear feature with increasing CO_{2bio} values during the night peaking between 07:00 and 08:00 UTC (i.e.

between 08:00 and 09:00 local time) can be observed. This buildup during the night can be explained by CO_2 from respiration fluxes accumulating in the stable and shallow nocturnal boundary layer. Then, after sunrise, the early morning CO_{2bio} peak starts to gradually decrease due to a combination of onset of photosynthesis and enhanced vertical mixing due to the growth of the boundary layer. At Beromünster, a decrease in CO_2 mixing ratios from both processes is visible more or less at the same time at the 212.5 m height level. As reported by Satar et al. (2016), this decrease in early morning CO_2 concentrations at the 212 m inlet is lagging the decrease at the lowest sampling level of 12.5 m by approximately one hor. Between 12:00 and 15:00 UTC, when the daytime convective boundary layer is fully established, the biospheric CO_2 continues to become more negative implying net photosynthetic uptake, which eventually stabilizes for 3 - 5 hours until nighttime CO_{2bio} accumulation starts.

4. Conclusions

From continuous measurements of CO and CO_2 and bi-weekly radiocarbon samples at the Beromünster tall tower, we have estimated a ΔCO to ΔCO_{2ff} ratio (R_{CO}) which was subsequently used to construct a 2.3-years long high-resolution CO_{2ff} time series. We have corrected the ratio for an offset of about 16 % caused by ^{14}C emissions from nearby NPPs. This bias was calculated by comparing the simulated mean enhancement in $\Delta^{14}C$ (1.6 ‰) due to NPPs with the measured mean depletion in $\Delta^{14}C$ due to fossil fuel CO_2 (9.9 ‰). The radiocarbon-based R_{CO} derived in this study during winter is about 30 % higher than the $CO:CO_2$ enhancement ratios estimated from continuous CO and CO_2 measurements during the same period, suggesting a significant biospheric contribution to regional CO_2 enhancements during this period. This is in agreement with previous studies that observed 20 - 30 % biospheric contribution during winter (Turnbull et al., 2011b).

538 The obtained CO_{2ff} time series shows a clear seasonality with frequent spikes during
539 winter associated with enhanced anthropogenic emissions and weak vertical mixing while
540 summer values are mostly stable.

541 By subtracting the estimated CO_{2ff} and CO_{2bg} from CO_{2meas}, we have also calculated
542 the biospheric CO_2 component, which ranges between -15 ppm and +30 ppm. Considering
543 only afternoon data (12:00 – 15:00 UTC) when the convective boundary layer is fully
544 established, CO_{2bio} showed its minimum in summer coinciding with net photosynthetic uptake
545 but still with frequent positive excursions especially during summer 2015 possibly driven by
546 the record high hot and dry summer during this period. During winter, CO_{2bio} becomes nearly
547 zero or positive, implying respiration fluxes.

548 A pronounced diurnal variation in CO_{2bio} was observed during summer modulated by
549 vertical mixing and biospheric exchange while this variation disappears during winter.
550 However, the variation in CO_{2bio} may also be influenced by the uncertainty of the CO_{2ff}
551 estimate especially due to applying a constant emission ratio while calculating CO_{2ff}. Hence,
552 it will be important in the future to include seasonally and diurnally resolved R_{CO} values from
553 high-frequency radiocarbon measurements to better estimate CO_{2ff}. Detailed analysis of the
554 PBL height may also provide useful information to better understand such variations and it
555 will be the focus of future studies. Additionally, including independent tracers such as
556 Atmospheric Potential Oxygen (APO) estimates based on concurrent CO_2 and O_2
557 measurements will be very useful to validate fossil-fuel emission estimates from the
558 radiocarbon method. This technique is also advantageous as the fossil fuel CO_2 estimate is
559 unaltered by contribution from NPPs as well as it accounts for the contribution from biofuels.
560
561
562

Acknowledgements

This project was funded by the Swiss National Science Foundation through the Sinergia project CarboCount CH (CRSII2 136273). We are also grateful to ICOS-Switzerland and the International Foundation High Alpine Research Stations Jungfraujoch and Gornergrat. The LARA laboratory would like to thank René Fischer for the production of large CO_2 amounts by combustion of the NIST standard oxalic acid II, and Dejan Husrefovic for the evaluation of the sample transfer line. Finally, we would like to thank Heather Graven and Nicolas Gruber for helpful input regarding radiocarbon emissions from NPPs and the Swiss Federal Nuclear Safety Inspectorate (ENSI) and the Berner Kraftwerke (BKW) for fruitful discussions and providing radiocarbon emission data.

588 List of Tables and Figures

589 Table 1. Ratios (R_{CO}) determined using radiocarbon measurements after correcting for
590 influence from NPPs and applying model II regression, and ratios derived from continuous
591 CO and CO_2 measurements by the CRDS analyzer as enhancements ($\Delta CO:\Delta CO_2$) using
592 Jungfraujoch background measurements. R_{CO} values are given in mmol/mol with standard
593 uncertainties of the slope and r^2 values in brackets and n represents the number of samples for
594 the radiocarbon method. Note that according to the Swiss emission inventory report for
595 greenhouse gas emissions in 2013, the annual anthropogenic CO/CO_2 emission ratio for the
596 national estimate is 7.8 mmol/mol.

	R_{CO} ($\Delta CO:\Delta CO_{2ff}$) (radiocarbon)	Number of samples (*n*)	$\Delta CO:\Delta CO_2$ (CRDS)
Winter (Dec-Feb)	12.5 ± 3.3 (0.6)	8	7.3 (0.9)
Summer (Jun-Aug)	14.1 ± 4.0 (0.3)	14	13.4 (0.02)
All data	13.4 ± 1.3 (0.6)	45	8.3 (0.5)

597

598

599

600

601

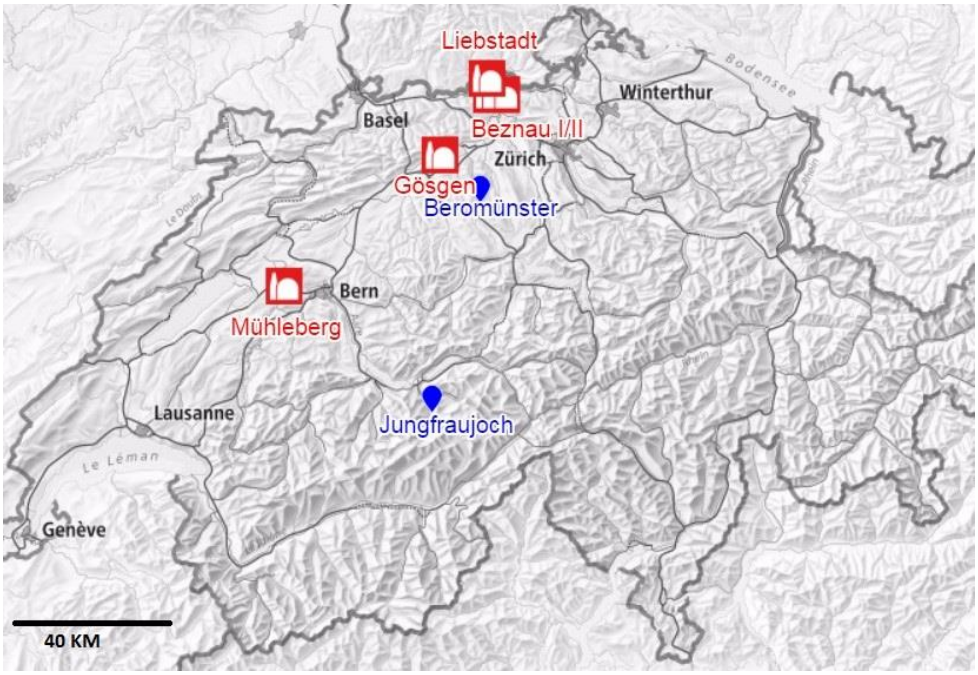

Figure 1. The geographical map of Beromünster and Jungfraujoch measurement sites (blue) as well as the five NPPs in Switzerland (red).

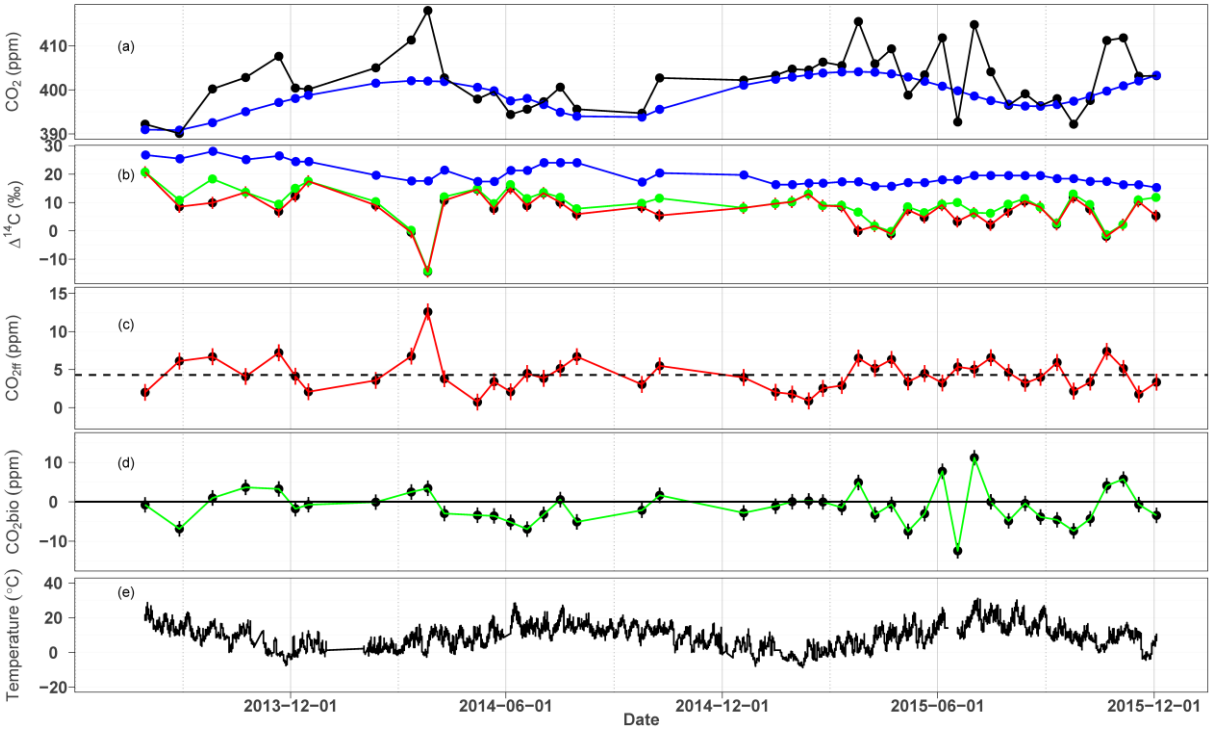

Figure 2. CO_2 mixing ratios (hourly averages) at Beromünster (black) from the sample inlet at 212.5 m and from background measurements at Jungfraujoch (blue) filtered using the REBS function for periods when ^{14}C sampling was conducted (a), $\Delta^{14}C$ determined from the bi-weekly point samplings at the site before (green) and after (red) correction for the intercomparison offset (see section 2.3) and the ^{14}C contribution from NPPs (see Eq. 5) and from 14-days integrated samplings at Jungfraujoch (blue) (b), CO_{2ff} determined during this period applying Eq. (4) with a mean CO_{2ff} value of 4.3 ppm (dashed line) (c), the biospheric CO_2 determined by simple subtraction of CO_{2bg} and CO_{2ff} from the CO_{2meas} (d), and the temperature record during this period at the 212.5 m height level (e). Error bars in (b) and (c) indicate the mean uncertainty in $\Delta^{14}C$ measurement (± 2.0 ‰) and calculated CO_{2ff} (± 1.2 ppm), averaged for the triplicate samples while error bars in (d) is obtained from error propagation of the components in (a), (b) and (c). CO_2 mixing ratios in the top panel are only shown from times matching the radiocarbon sampling at Beromünster tower.

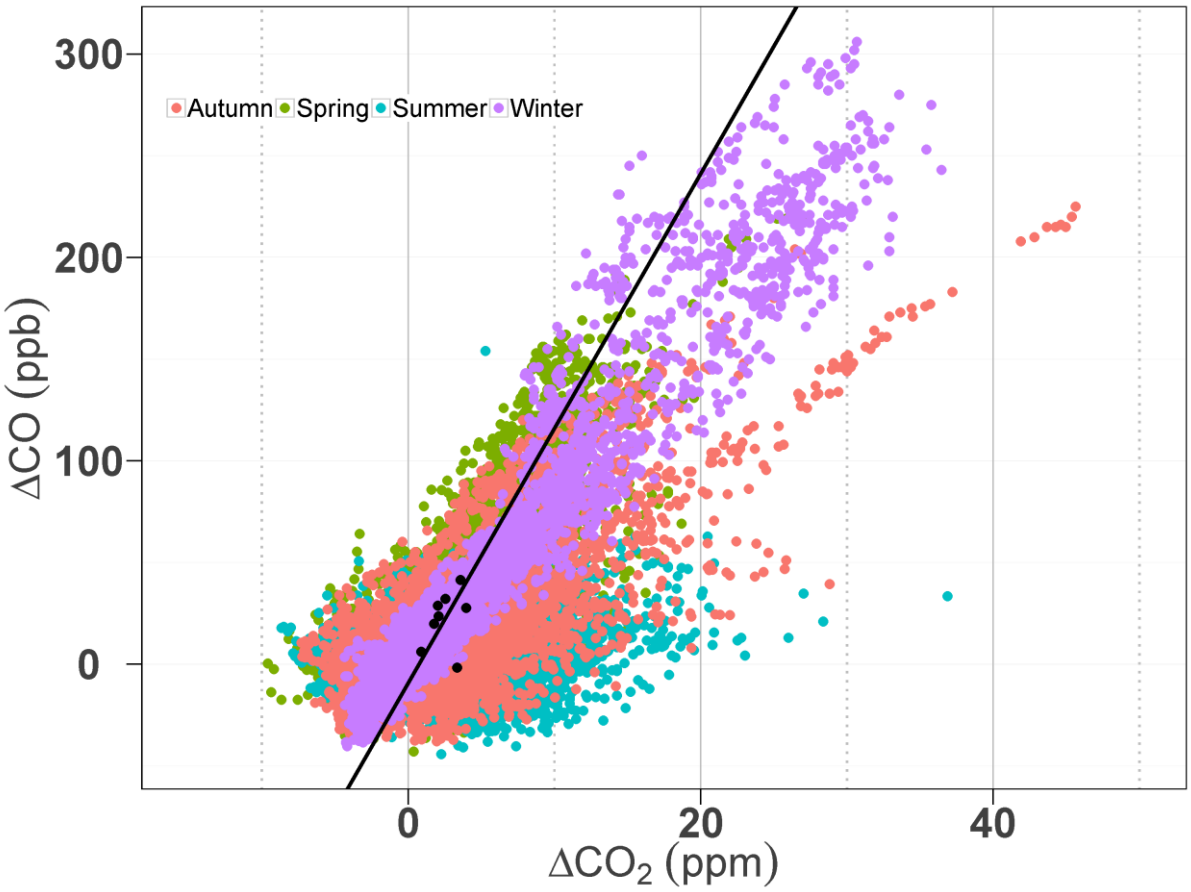

Figure 3. The correlation between enhancements in CO and CO_2 at Beromünster over Jungfraujoch background for the different seasons. The black dots and the black solid line correspond to the individual wintertime R_{CO} values and the linear fit to these points, respectively.

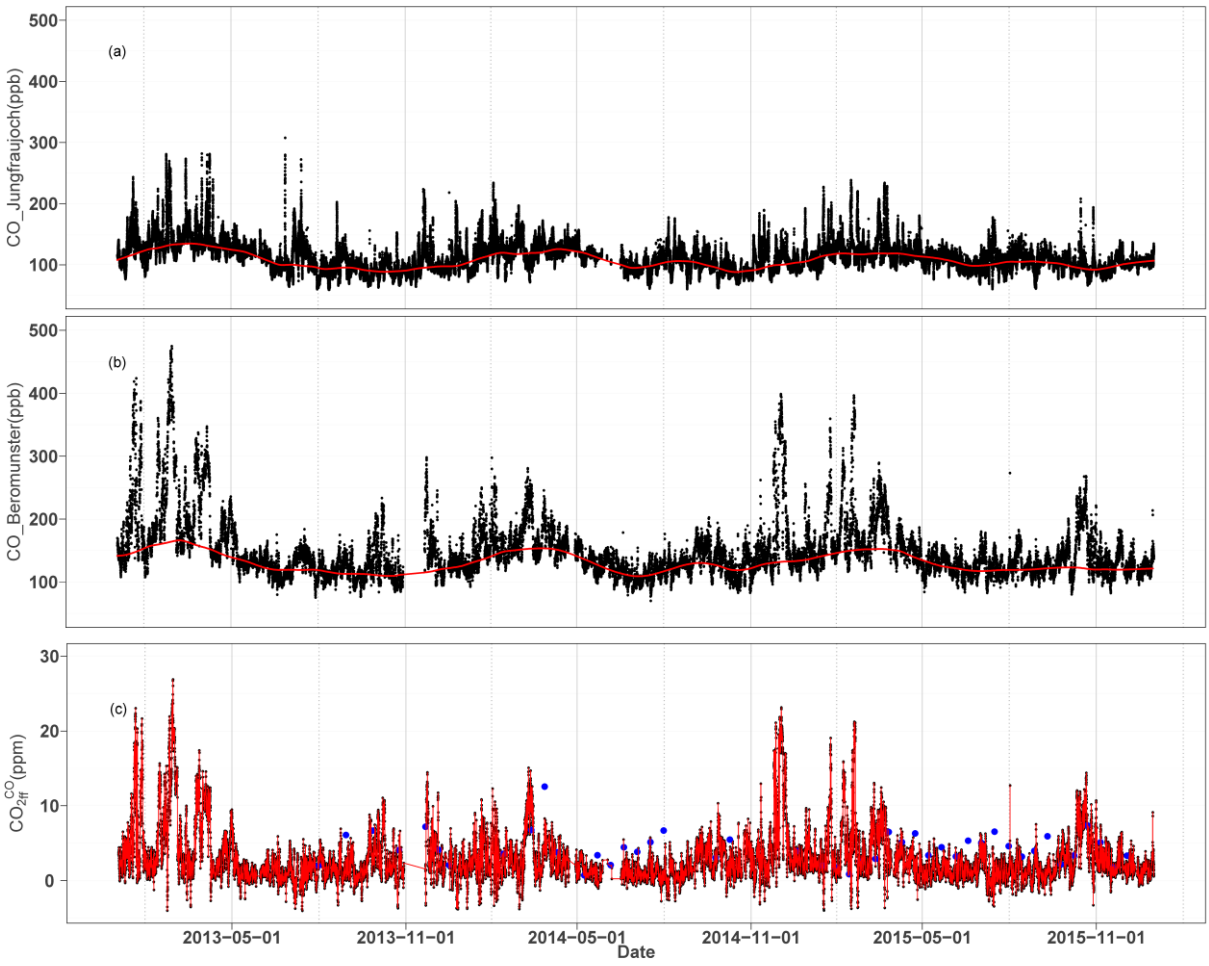

Figure 4. Time series of hourly mean CO mixing ratios measured at Jungfraujoch (a) and Beromünster (b) sites with the red curve showing the estimated background values using the REBS method with 60 days window. Panel (c) shows the hourly mean CO_{2ff} time series calculated using the emission ratios determined from radiocarbon measurements, and the CO enhancements at Beromünster over the Jungfraujoch background based on Eq. (7). The blue dots in panel C shows the CO_{2ff} values determined using the radiocarbon measurements.

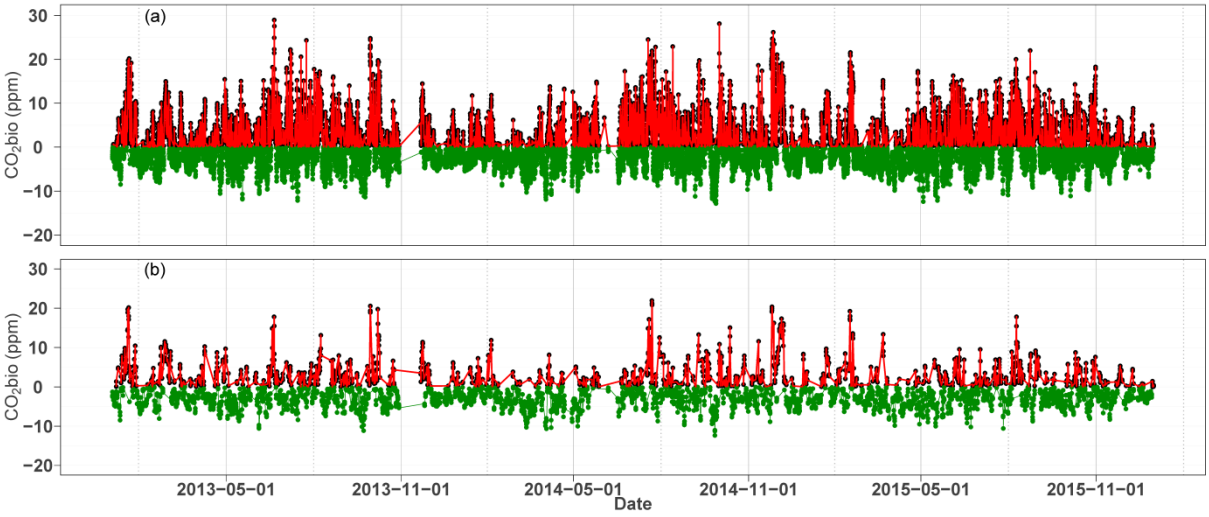

Figure 5. Time series (hourly resolution) of the biospheric CO_2 derived as a residual of the difference between the total CO_2, CO_{2bg} and CO_{2ff} for all data (a), and only afternoon data from 12:00-15:00 UTC (b). The green lines show negative CO_{2bio} implying uptake while red ones represent positive CO_{2bio}. The average uncertainty of CO_{2bio} amounts ±1.3 ppm calculated from error propagation.

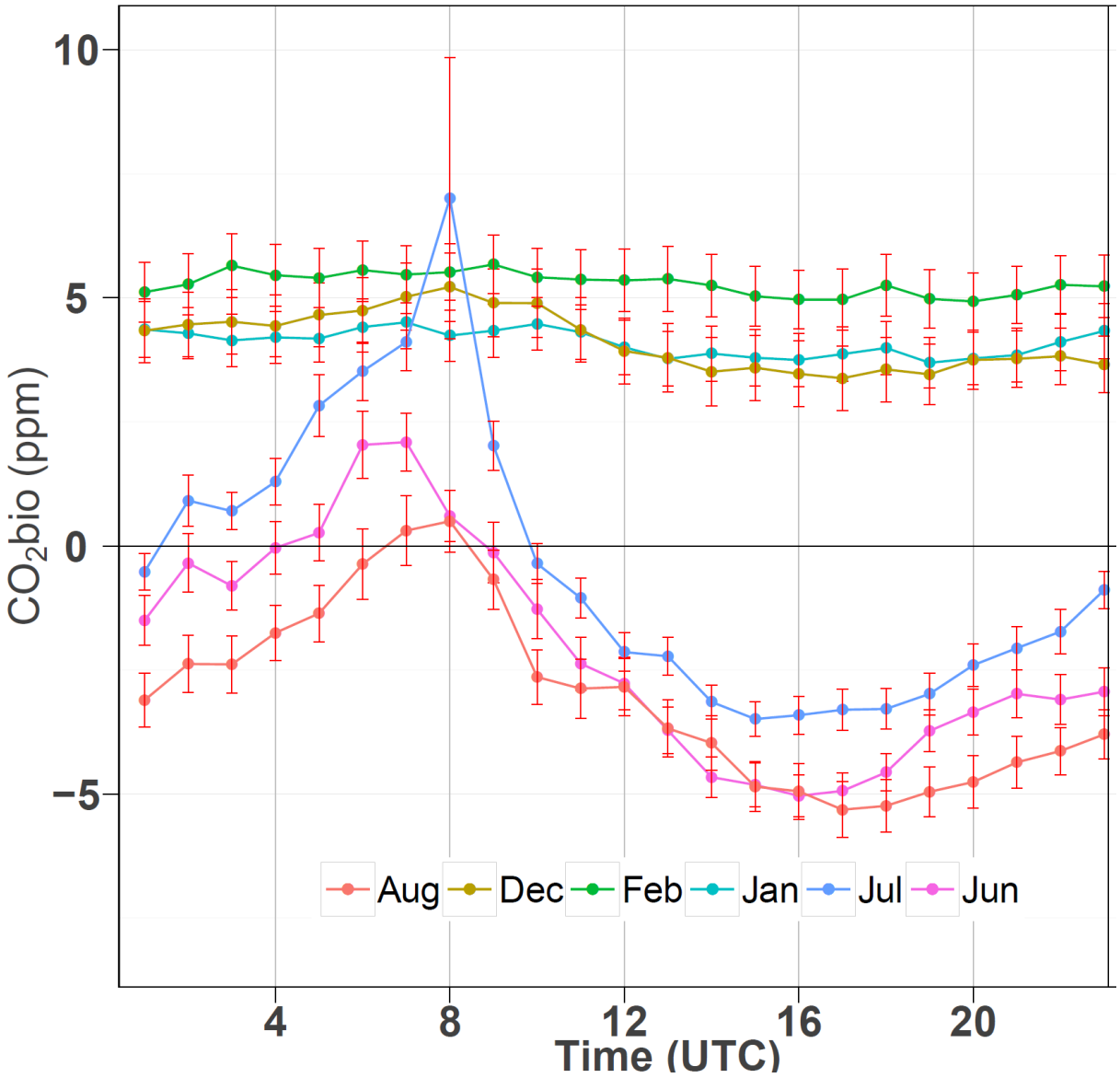

Figure 6. Hourly variations of monthly averaged biospheric CO_2 during summer (Jun – Aug) and winter (Dec – Feb). While winter values dominated by respiration are constant throughout a day, summer values show a significant diurnal variation induced by photosynthesis and vertical mixing. The error bars are the standard deviations of the hourly averaged CO_{2bio} values for each month.

667 **References**

668 Ballantyne, A. P., Andres, R., Houghton, R., Stocker, B. D., Wanninkhof, R., Anderegg, W., Cooper, L.
669 A., DeGrandpre, M., Tans, P. P., Miller, J. B., Alden, C., and White, J. W. C.: Audit of the global carbon
670 budget: estimate errors and their impact on uptake uncertainty, Biogeosciences, 12, 2565-2584,
671 10.5194/bg-12-2565-2015, 2015.

672 Basu, S., Miller, J. B., and Lehman, S.: Separation of biospheric and fossil fuel fluxes of CO_2 by
673 atmospheric inversion of CO_2 and $^{14}CO_2$ measurements: Observation System Simulations, Atmos
674 Chem Phys, 16, 5665-5683, 10.5194/acp-16-5665-2016, 2016.

675 Berhanu, T. A., Satar, E., Schanda, R., Nyfeler, P., Moret, H., Brunner, D., Oney, B., and Leuenberger,
676 M.: Measurements of greenhouse gases at Beromünster tall tower station in Switzerland, Atmos.
677 Meas. Tech. , 9, 10.5194/amt-9-2603-2016, 2016.

678 Ciais, P., Paris, J. D., Marland, G., Peylin, P., Piao, S. L., Levin, I., Pregger, T., Scholz, Y., Friedrich, R.,
679 Rivier, L., Houwelling, S., Schulze, E. D., and Team, C. S.: The European carbon balance. Part 1: fossil
680 fuel emissions, Glob Change Biol, 16, 1395-1408, DOI 10.1111/j.1365-2486.2009.02098.x, 2010.

681 Currie, L. A.: The remarkable metrological history of radiocarbon dating [II], J Res Natl Inst Stan, 109,
682 185-217, 10.6028/jres.109.013, 2004.

683 FOEN: Switzerland's Informative Inventory Report 2015, Swiss Federal Office for the Environement
684 2015a.

685 FOEN: Switzerland's Greenhose Gas Inventory 1990-2013, Swiss Federal Office for the Environment
686 2015b.

687 Friedlingstein, P., Houghton, R. A., Marland, G., Hackler, J., Boden, T. A., Conway, T. J., Canadell, J. G.,
688 Raupach, M. R., Ciais, P., and Le Quere, C.: Update on CO_2 emissions, Nat Geosci, 3, 811-812, Doi
689 10.1038/Ngeo1022, 2010.

690 Gamnitzer, U., Karstens, U., Kromer, B., Neubert, R. E. M., Meijer, H. A. J., Schroeder, H., and Levin, I.:
691 Carbon monoxide: A quantitative tracer for fossil fuel CO_2?, J Geophys Res-Atmos, 111, Artn D22302

692 Doi 10.1029/2005jd006966, 2006.
693 Graven, H. D., Guilderson, T. P., and Keeling, R. F.: Methods for high-precision C-14 AMS
694 measurement of atmospheric CO2 at LLNL, Radiocarbon, 49, 349-356, 2007.
695 Graven, H. D., and Gruber, N.: Continental-scale enrichment of atmospheric $^{14}CO_2$ from the nuclear
696 power industry: potential impact on the estimation of fossil fuel-derived CO_2, Atmos. Chem. Phys.,
697 11, 12339-12349, 10.5194/acp-11-12339-2011, 2011.
698 Hammer, S., Friedrich, R., Kromer, B., Cherkinsky, A., Lehman, S. J., Meijer, H. A. J., Nakamura, T.,
699 Palonen, V., Reimer, R. W., Smith, A. M., Southon, J. R., Szidat, S., Turnbull, J., and Uchida, M.:
700 Compatibility of Atmospheric $^{14}CO_2$ Measurements: Comparing the Heidelberg Low-Level Counting
701 Facility to International Accelerator Mass Spectrometry (AMS) Laboratories, Radiocarbon, 1-9,
702 10.1017/RDC.2016.62, 2016.
703 Heimann, M., and Reichstein, M.: Terrestrial ecosystem carbon dynamics and climate feedbacks,
704 Nature, 451, 289-292, 10.1038/nature06591, 2008.
705 Henne, S., Brunner, D., Oney, B., Leuenberger, M., Eugster, W., Bamberger, I., Meinhardt, F.,
706 Steinbacher, M., and Emmenegger, L.: Validation of the Swiss methane emission inventory by
707 atmospheric observations and inverse modelling, Atmos Chem Phys, 16, 3683-3710, 2016.
708 Le Quéré, C., Andrew, R. M., Canadell, J. G., Sitch, S., Korsbakken, J. I., Peters, G. P., Manning, A. C.,
709 Boden, T. A., Tans, P. P., Houghton, R. A., Keeling, R. F., Alin, S., Andrews, O. D., Anthoni, P., Barbero,
710 L., Bopp, L., Chevallier, F., Chini, L. P., Ciais, P., Currie, K., Delire, C., Doney, S. C., Friedlingstein, P.,
711 Gkritzalis, T., Harris, I., Hauck, J., Haverd, V., Hoppema, M., Klein Goldewijk, K., Jain, A. K., Kato, E.,
712 Körtzinger, A., Landschützer, P., Lefèvre, N., Lenton, A., Lienert, S., Lombardozzi, D., Melton, J. R.,
713 Metzl, N., Millero, F., Monteiro, P. M. S., Munro, D. R., Nabel, J. E. M. S., Nakaoka, S. I., O'Brien, K.,
714 Olsen, A., Omar, A. M., Ono, T., Pierrot, D., Poulter, B., Rödenbeck, C., Salisbury, J., Schuster, U.,
715 Schwinger, J., Séférian, R., Skjelvan, I., Stocker, B. D., Sutton, A. J., Takahashi, T., Tian, H., Tilbrook, B.,

van der Laan-Luijkx, I. T., van der Werf, G. R., Viovy, N., Walker, A. P., Wiltshire, A. J., and Zaehle, S.: Global Carbon Budget 2016, Earth Syst. Sci. Data, 8, 605-649, 10.5194/essd-8-605-2016, 2016.

Leuenberger, M. C., Eyer, M., Nyfeler, P., Stauffer, B., and Stocker, T. F.: High-resolution ^{13}C measurements on ancient air extracted from less than 10 cm(3) of ice, Tellus B, 55, 138-144, DOI 10.1034/j.1600-0889.2003.01463.x, 2003.

Levin, I., Kromer, B., Schmidt, M., and Sartorius, H.: A novel approach for independent budgeting of fossil fuel CO_2 over Europe by $^{14}CO_2$ observations, Geophys Res Lett, 30, Doi 10.1029/2003gl018477, 2003.

Levin, I., and Karstens, U.: Inferring high-resolution fossil fuel CO_2 records at continental sites from combined $^{14}CO_2$ and CO observations, Tellus B, 59, 245-250, DOI 10.1111/j.1600-0889.2006.00244.x, 2007.

Levin, I., Naegler, T., Kromer, B., Diehl, M., Francey, R. J., Gomez-Pelaez, A. J., Steele, L. P., Wagenbach, D., Weller, R., and Worthy, D. E.: Observations and modelling of the global distribution and long-term trend of atmospheric (CO2)-C-14 (vol 62, pg 26, 2010), Tellus B, 62, 207-207, 10.1111/j.1600-0889.2010.00456.x, 2010.

Levin, I., Kromer, B., and Hammer, S.: Atmospheric Delta $^{14}CO_2$ trend in Western European background air from 2000 to 2012, Tellus B, 65, DOI 10.3402/tellusb.v65i0.20092, 2013.

Loosli, H. H., and Oeschger, H.: C-14 in the Environment of Swiss Nuclear Installations, Radiocarbon, 31, 747-753, 1989.

Lopez, M., Schmidt, M., Delmotte, M., Colomb, A., Gros, V., Janssen, C., Lehman, S. J., Mondelain, D., Perrussel, O., Ramonet, M., Xueref-Remy, I., and Bousquet, P.: CO, NOx and $^{13}CO_2$ as tracers for fossil fuel CO_2: results from a pilot study in Paris during winter 2010, Atmos Chem Phys, 13, 7343-7358, DOI 10.5194/acp-13-7343-2013, 2013.

739 Manning, M. R., Lowe, D. C., Melhuish, W. H., Sparks, R. J., Wallace, G., Brenninkmeijer, C. A. M., and
740 Mcgill, R. C.: The Use of Radiocarbon Measurements in Atmospheric Studies, Radiocarbon, 32, 37-58,
741 1990.
742 Marland, G.: Uncertainties in accounting for CO_2 from fossil fuels, J Ind Ecol, 12, 136-139, DOI
743 10.1111/j.1530-9290.2008.00014.x, 2008.
744 Marland, G., Hamal, K., and Jonas, M.: How Uncertain Are Estimates of CO_2 Emissions ?, J Ind Ecol,
745 13, 4-7, DOI 10.1111/j.1530-9290.2009.00108.x, 2009.
746 MeteoSuisse: Bulletin climatologique été 2015, 2015.
747 Naegler, T., and Levin, I.: Observation-based global biospheric excess radiocarbon inventory 1963–
748 2005, Journal of Geophysical Research: Atmospheres, 114, n/a-n/a, 10.1029/2008JD011100, 2009.
749 Nemec, M., Wacker, L., and Gaggeler, H.: Optimization of the Graphitization Process at Age-1,
750 Radiocarbon, 52, 1380-1393, 2010.
751 Oney, B., Henne, S., Gruber, N., Leuenberger, M., Bamberger, I., Eugster, W., and Brunner, D.: The
752 CarboCount CH sites: characterization of a dense greenhouse gas observation network, Atmos.
753 Chem. Phys., 15, 11147-11164, 10.5194/acp-15-11147-2015, 2015.
754 Oney, B., Gruber, N., Henne, S., Leuenberger, M., and Brunner, D.: A CO-based method to determine
755 the regional biospheric signal in atmospheric, Tellus B: Chemical and Physical Meteorology, 69,
756 1353388, 10.1080/16000889.2017.1353388, 2017.
757 Orth, R., Zscheischler, J., and Seneviratne, S. I.: Record dry summer in 2015 challenges precipitation
758 projections in Central Europe, Scientific Reports, 6, 28334, 10.1038/srep28334, 2016.
759 Peylin, P., Houweling, S., Krol, M. C., Karstens, U., Rödenbeck, C., Geels, C., Vermeulen, A., Badawy,
760 B., Aulagnier, C., Pregger, T., Delage, F., Pieterse, G., Ciais, P., and Heimann, M.: Importance of fossil
761 fuel emission uncertainties over Europe for CO_2 modeling: model intercomparison, Atmos. Chem.
762 Phys., 11, 6607-6622, 10.5194/acp-11-6607-2011, 2011.

763 Popa, M. E., Vollmer, M. K., Jordan, A., Brand, W. A., Pathirana, S. L., Rothe, M., and Rockmann, T.:
764 Vehicle emissions of greenhouse gases and related tracers from a tunnel study: CO: CO2, N2O: CO2,
765 CH4 : CO2, O-2 : CO2 ratios, and the stable isotopes C-13 and O-18 in CO2 and CO, Atmos Chem Phys,
766 14, 2105-2123, 10.5194/acp-14-2105-2014, 2014.
767 Ruckstuhl, A. F., Henne, S., Reimann, S., Steinbacher, M., Vollmer, M. K., O'Doherty, S., Buchmann, B.,
768 and Hueglin, C.: Robust extraction of baseline signal of atmospheric trace species using local
769 regression, Atmos Meas Tech, 5, 2613-2624, DOI 10.5194/amt-5-2613-2012, 2012.
770 Satar, E., Berhanu, T. A., Brunner, D., Henne, S., and Leuenberger, M.: Continuous CO2/CH4/CO
771 measurements (2012–2014) at Beromünster tall tower station in Switzerland, Biogeosciences, 13,
772 2623-2635, 10.5194/bg-13-2623-2016, 2016.
773 Schibig, M. F., Mahieu, E., Henne, S., Lejeune, B., and Leuenberger, M. C.: Intercomparison of in situ
774 NDIR and column FTIR measurements of CO_2 at Jungfraujoch, Atmos Chem Phys, 16, 9935-9949,
775 10.5194/acp-16-9935-2016, 2016.
776 Szidat, S., Salazar, G. A., Vogel, E., Battaglia, M., Wacker, L., Synal, H. A., and Turler, A.: ^{14}C Analysis
777 and Sample Preparation at the New Bern Laboratory for the Analysis of Radiocarbon with AMS
778 (LARA), Radiocarbon, 56, 561-566, 10.2458/56.17457, 2014.
779 Tolk, L. F., Meesters, A. G. C. A., Dolman, A. J., and Peters, W.: Modelling representation errors of
780 atmospheric CO_2 mixing ratios at a regional scale, Atmos. Chem. Phys., 8, 6587-6596, 10.5194/acp-8-
781 6587-2008, 2008.
782 Turnbull, J., Rayner, P., Miller, J., Naegler, T., Ciais, P., and Cozic, A.: On the use of $^{14}CO_2$ as a tracer for
783 fossil fuel CO_2: Quantifying uncertainties using an atmospheric transport model, J Geophys Res-
784 Atmos, 114, 10.1029/2009jd012308, 2009.
785 Turnbull, J. C., Miller, J. B., Lehman, S. J., Tans, P. P., Sparks, R. J., and Southon, J.: Comparison of
786 $^{14}CO_2$, CO, and SF6 as tracers for recently added fossil fuel CO_2 in the atmosphere and implications for
787 biological CO_2 exchange, Geophys Res Lett, 33, Doi 10.1029/2005gl024213, 2006.

788 Turnbull, J. C., Karion, A., Fischer, M. L., Faloona, I., Guilderson, T., Lehman, S. J., Miller, B. R., Miller,
789 J. B., Montzka, S., Sherwood, T., Saripalli, S., Sweeney, C., and Tans, P. P.: Assessment of fossil fuel
790 carbon dioxide and other anthropogenic trace gas emissions from airborne measurements over
791 Sacramento, California in spring 2009, Atmos Chem Phys, 11, 705-721, 10.5194/acp-11-705-2011,
792 2011.
793 Turnbull, J. C., Keller, E. D., Baisden, T., Brailsford, G., Bromley, T., Norris, M., and Zondervan, A.:
794 Atmospheric measurement of point source fossil CO_2 emissions, Atmos Chem Phys, 14, 5001-5014,
795 DOI 10.5194/acp-14-5001-2014, 2014.
796 Turnbull, J. C., Sweeney, C., Karion, A., Newberger, T., Lehman, S. J., Tans, P. P., Davis, K. J., Lauvaux,
797 T., Miles, N. L., Richardson, S. J., Cambaliza, M. O., Shepson, P. B., Gurney, K., Patarasuk, R., and
798 Razlivanov, I.: Toward quantification and source sector identification of fossil fuel CO_2 emissions from
799 an urban area: Results from the INFLUX experiment, J Geophys Res-Atmos, 120, 292-312, Doi
800 10.1002/2014jd022555, 2015.
801 Vogel, F. R., Hammer, S., Steinhof, A., Kromer, B., and Levin, I.: Implication of weekly and diurnal ^{14}C
802 calibration on hourly estimates of CO-based fossil fuel CO_2 at a moderately polluted site in
803 southwestern Germany, Tellus B, 62, 512-520, DOI 10.1111/j.1600-0889.2010.00477.x, 2010.
804 Wacker, L., Christl, M., and Synal, H. A.: Bats: A new tool for AMS data reduction, Nucl Instrum Meth
805 B, 268, 976-979, 10.1016/j.nimb.2009.10.078, 2010.
806 Yim, M. S., and Caron, F.: Life cycle and management of carbon-14 from nuclear power generation,
807 Prog Nucl Energ, 48, 2-36, 10.1016/j.pnucene.2005.04.002, 2006.
808 Zellweger, C., Huglin, C., Klausen, J., Steinbacher, M., Vollmer, M., and Buchmann, B.: Inter-
809 comparison of four different carbon monoxide measurement techniques and evaluation of the long-
810 term carbon monoxide time series of Jungfraujoch, Atmos Chem Phys, 9, 3491-3503, 2009.

811 Zellweger, C., Steinbacher, M., and Buchmann, B.: Evaluation of new laser spectrometer techniques
812 for in-situ carbon monoxide measurements, Atmos Meas Tech, 5, 2555-2567, 10.5194/amt-5-2555-
813 2012, 2012.
814 Zondervan, A., and Meijer, H. A. J.: Isotopic characterisation of CO_2 sources during regional pollution
815 events using isotopic and radiocarbon analysis, Tellus B, 48, 601-612, DOI 10.1034/j.1600-
816 0889.1996.00013.x, 1996.

817

818

819

820